Magnetic helicity and energy budgets of jet events from an emerging solar active region

A. Nindos[1], S. Patsourakos[1], K. Moraitis[1], V. Archontis[1], E. Liokati[1], M. K. Georgoulis[2,3], A. A. Norton[4]

[1]Section of Astrogeophysics, Department of Physics, University of Ioannina, 45110 Ioannina, Greece
[2]The Johns Hopkins University Applied Physics Laboratory, Laurel, MD, 20723, USA
[3]Research Center for Astronomy and Applied Mathematics, Academy of Athens, Athens, 11527, Greece
[4]HEPL Solar Physics, Stanford University, 94305-4085, Stanford, CA, USA

Abstract. Using photospheric vector magnetograms obtained by the Helioseismic and Magnetic Imager on board the Solar Dynamics Observatory and a magnetic connectivity-based method, we compute the magnetic helicity and free magnetic energy budgets of a simple bipolar solar active region (AR) during its magnetic flux emergence phase which lasted ~47 hrs. The AR did not produce any coronal mass ejections (CMEs) or flares with an X-ray class above C1.0 but it was the site of 60 jet events during its flux emergence phase. The helicity and free energy budgets of the AR were below established eruption-related thresholds throughout the interval we studied. However, in addition to their slowly-varying evolution, each of the time profiles of the helicity and free energy budgets showed discrete localized peaks, with eight pairs of them occurring at times of jets emanating from the AR. These jets featured larger base areas and longer durations than the other jets of the AR. We estimated, for the first time, the helicity and free magnetic energy changes associated with these eight jets which were in the ranges of 0.5-7.1 x 10^{40} Mx^2 and 1.1-6.9 x 10^{29} erg, respectively. Although these values are one to two orders of magnitude smaller than those usually associated with CMEs, the relevant percentage changes were significant and ranged from 13% to 76% for the normalized helicity and from 9% to 57% for the normalized free magnetic energy. Our study indicates that occasionally jets may have a significant imprint in the evolution of helicity and free magnetic energy budgets of emerging active regions. **This presentation is based on a paper which has been recently accepted to A&A (Letters). The accepted version of the paper can be downloaded from https://arxiv.org/pdf/2409.00931**

1. Introduction

Solar jets are collimated ejections of plasma that is launched outward along magnetic field lines. They occur prolifically in diverse environments such as coronal holes, the quiet Sun, and active regions (ARs) and are observed in different wavebands, most notably soft X-rays, EUV, and Hα, in the latter case being called surges.

There is a tradition of studying energetic magnetic phenomena in terms of their magnetic free energy, E_f, and helicity, H, of the magnetic field. Older and more recent results indicate that active regions (ARs) tend to produce eruptive flares when they accumulate significant budgets of both magnetic free energy and helicity.

Contrary to flares and CMEs, there is only a small number of publications discussing how the occurrence of jets is related to the helicity budget of their source regions: see the numerical experiments by Linan et al. (2018) and Pariat et al. (2023) and also the work by Green et al. (2023) who monitored the evolution of the helicity index (ratio of the magnetic helicity of the current-carrying field to the total magnetic helicity) in a large emerging eruptive active region and found that some major jets occurred at time intervals when the helicity index obtained large values.

Here we present the evolution of magnetic helicity and free magnetic energy in an AR that produced several jet events during its flux emergence phase. We show, for the first time with such clarity, that several of these jets occurred at times when both magnetic helicity and free energy showed distinct localized peaks and calculate the helicity and free magnetic energy changes associated with these jets.

2. Observations and data reduction

We study emerging AR NOAA 11096. The magnetic helicity and free magnetic budgets of the AR were calculated using HMI vector magnetograms. More specifically, we used the "hmi.sharp_cea_720s_dconS" data series which provides Lambert cylindrical equal-area (CEA) projections of the photospheric magnetic field vector that were corrected for scattered light.

At each timestamp we computed the instantaneous free magnetic energy and helicity budgets using the connectivity-based (CB) method of Georgoulis et al. (2012). The input of this method is a single vector magnetogram which is partitioned to yield a connectivity matrix populated by the magnetic flux associated with connections between partitions of opposite polarities. This collection of connection is treated as an ensemble of force-free flux tubes each with known footpoints, force-free parameter, and flux.

The results from the CB method were compared with results from the flux-integration (FI) method: in it the magnetic helicity and energy fluxes across the photospheric boundary are computed. The inputs of this method are the normal and tangential components of the photospheric magnetic field as well as the cross-field velocity field at the photosphere.

The jets associated with the AR were identified in 211 Å images from the Atmospheric Imaging Assembly (AIA) telescope onboard SDO. This AIA channel is sensitive to 2 MK plasmas. We degraded the cadence of our AIA datacube from 11 s to 2 min.

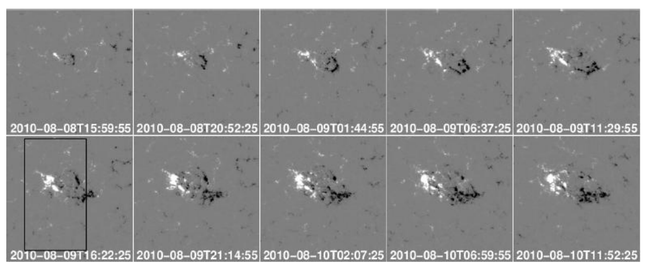

Fig. 1. *Selected HMI line-of-sight magnetograms showing the evolution of the photospheric magnetic field in AR11096. In each image the field of view is 205" x 205". The black box shows the area that is displayed in Fig. 2.*

3. Results

AR11096 emerged in an area without pre-existing ARs (see Fig. 1 for characteristic snapshots). The AR produced several jets, most of which occurred during its emergence phase. Therefore we limited our calculations to the flux emergence phase of the AR which lasted ~47 hours.

Fig. 1 indicates that AR11096 was a simple bipolar AR. The AR produced neither CMEs nor flares with an X-ray class above C1.0 (see Liokati et al. 2022, and also the time profile of the 211-Å flux from the AR in Fig. 3(a)). During the interval we studied, several jets emanated from the AR, most of them from its eastern part. We identified 60 jets which is probably a lower limit because the cadence of the AIA data we used was 2 min. Characteristic snapshots of major jets hosted by the AR are given in Fig. 2.

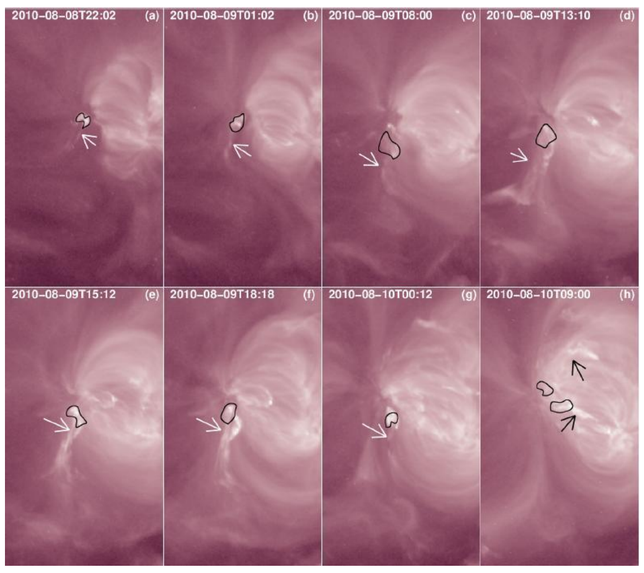

Fig. 2. *Selected 211-Å AIA images showing the jets (denoted by arrows) that were associated with localized peaks of the free magnetic energy and helicity budgets of AR11096. Contours outline the calculated apparent areas of the bases of the jets. The field of view is 103" x 181" and corresponds to the black box of Fig. 1.*

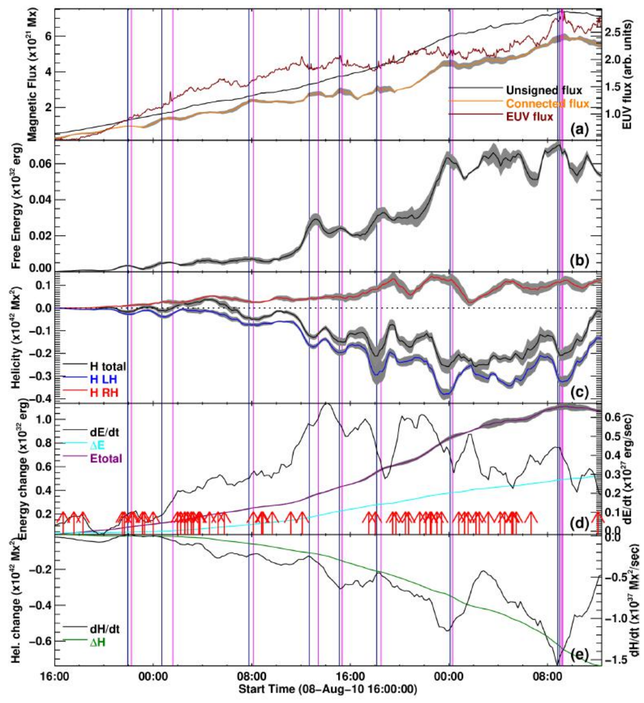

Fig. 3. *Top: Evolution of magnetic properties of AR11096. (a) Unsigned magnetic flux, unsigned connected magnetic flux used in the CB method, and EUV flux of the AR resulted from AIA's 211 Å channel (black, yellow, and maroon curves, respectively). (b) Free magnetic energy. (c) Net, left-handed, and right-handed helicity (black, blue, and red curves, respectively). (d) Total magnetic energy from the CB method, magnetic energy injection rate from the FI method and the corresponding accumulated magnetic energy (purple, black, and cyan curves, respectively). (e) Helicity injection rate from the FI method and the corresponding accumulated helicity (black and green curves, respectively). Vertical dark blue and pink lines show the start and end times of major jet events while arrows indicate the start time of the remaining jets of the AR. Error bars are indicated by the gray bands.*

In Fig. 3 we give the time profiles of the free magnetic energy (E_f , panel b) and magnetic helicity (panel c) of the AR. The evolution of the injection rates of magnetic energy, dE/dt, and helicity, dH/dt, from the FI method as well as the resulting accumulated quantities (ΔE and ΔH, respectively) are given in panels (d) and (e) of Fig. 3.

A direct comparison between the results from the CB-method and the results from the FI-method is not possible. However, Fig. 3 indicates that there is a very good resemblance between the evolution of ΔE and the evolution of the total magnetic energy, E_{tot}, derived from the CB method (correlation coeffcient of 0.96). The correlation coeffcient between ΔH and the net helicity from the CB-method is 0.75, i.e. rather strong but weaker than that of the ΔE-E_{tot} pair.

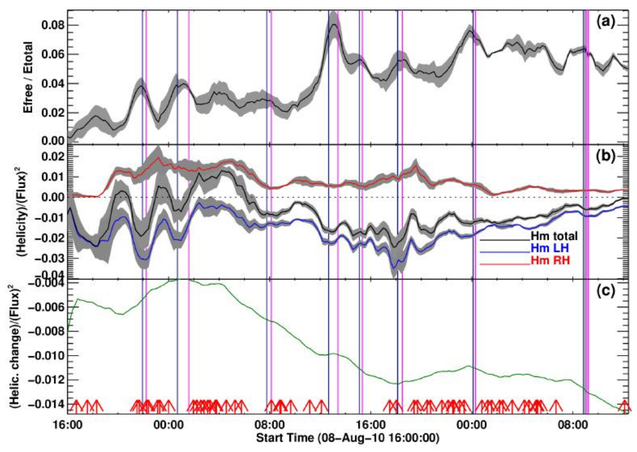

Fig. 4. *Evolution of normalized magnetic quantities for AR11096. (a) Ratio of the free magnetic energy to the total magnetic energy. (b) Ratios of the net, left-handed, and right-handed helicity to the connected magnetic flux squared (black, blue, and red curves, respectively). (c) Ratio of the accumulated helicity from the FI method to the connected magnetic flux squared. Vertical lines and arrows are as in Fig. 3.*

The free magnetic energy and helicity budgets of the AR are always clearly below reported thresholds for the occurrence of major flares; compare the values appearing in panels (b) and (c) of Fig. 3 with the thresholds of 4 x 10^{31} erg and 2 x 10^{42} Mx^2, respectively, established by Tziotziou et al. (2012). The accumulated budgets of ΔE and ΔH resulting from the FI-method (see panels (d) and (e) of Fig. 3) are also lower than the corresponding thresholds established by Liokati et al. (2022) (2 x 10^{32} erg and 9 x 10^{41} Mx^2, respectively).

The slowly-varying trends of the free magnetic energy and helicity budgets are paired with shorter localized peaks (see Fig. 3(b, c)). In eight cases these peaks are synchronized with jets produced in the AR. This is evident in Fig. 3 where the start and end times of major jet events produced in the AR are marked by dark blue and pink vertical lines, respectively. The localized peaks associated with the occurrence of jets appear cotemporally in the free magnetic energy, net helicity, H, and left-handed helicity (H_{LH}) curves. With the probable exception of the seventh event, their signature is not prominent in the right-handed helicity (H_{RH}) curve (that is, the minority sense of helicity). Furthermore, all the E_f -H localized peaks occurring in conjuction with jets stand out beyond error bars (the latter are indicated by the gray bands of Fig. 3 and result from the standard deviations of the moving five-point averages of the pertinent curves).

Most of these localized E_f and H peaks occur either around the start time of a major jet (peaks 1, 3, and 5) or between the start and end time of a major jet (events 2, 4) while for the others, small temporal offsets can be registered between the E_f-H peaks and the interval of occurrence of the jet. These offsets were on the order of 12-24 min and consequently they were barely resolved because the cadence of the magnetograms was 12 min.

Panels (d) and (e) of Fig. 3 indicate that the occurrence of events 1-8 was not associated with any prominent signature in the ΔE and ΔH curves. However, the dE/dt curve shows local peaks associated with events 3, 4, and 8 while the dH/dt curve shows absolute value local peaks associated with events 3, 5, 7, and 8.

In Fig. 4 we present the evolution of the ratio of E_f to the total magnetic energy, E_f/E_{tot}, as well as the connected-magnetic-flux normalized helicities (H/Φ^2_{conn}, H_{RH}/Φ^2_{conn}, H_{LH}/Φ^2_{conn}). The values of these curves are a factor of ~2 lower than those associated with the two large eruptive ARs studied by Liokati et al. (2023). However, the normalized parameters of the free energy and helicity exhibit well-defined local peaks that are associated with jet events 1-8.

Returning in Fig. 3, the free magnetic energy and helicity changes (DE_f and DH, respectively) associated with events 1-8 were calculated as the difference between the relevant localized peak and the value at the curve's point of inflection occurring just after the localized peak. The results appear in columns 2 and 4 of Table 1. The corresponding percentages of the normalized E_f and H losses (see Fig. 4) are given in columns 3 and 5 of Table 1.

Table 1: Free magnetic energy and helicity budgets of jet events.

Event Number	DE_f ($\times 10^{29}$ erg)	(%)	DH ($\times 10^{40}$ Mx^2)	(%)
1	-1.9	-57	1.3	-76
2	-1.4	-26	0.5	-40
3	-1.1	-15	1.7	-35
4	-7.9	-27	3.9	-31
5	-3.9	-15	4.0	-27
6	-2.9	-9	5.6	-26
7	-5.5	-18	3.4	-13
8	-6.9	-14	7.1	-34

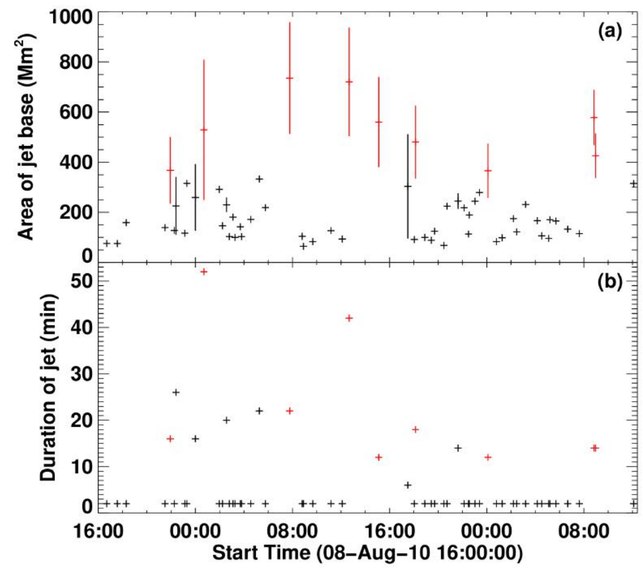

Fig. 5. *(a) Apparent areas of the bases of all jet events. When possible the measurements are accompanied with their uncertainties. (b) Duration of jets. The duration of those jets that appeared in only one AIA image has been set to 2 min. In both panels red symbols correspond to the events presented in Fig. 2 while black symbols are used for the other events. Each symbol has been placed at the start time of the corresponding jet.*

In addition to the jet events that were associated with localized peaks in the E_f and H budgets of the AR, several other jets were also produced in the AR (denoted by the arrows in Figs. 3 and 4). The duration of these jets was short (see Fig. 5(b)) and neither of them coincided with localized peaks appearing in both the E_f and H time profiles. We investigated how the former group of jets can be further distinguished from the latter. To this end, we calculated the apparent area of the bases of all jets. The results appear in Fig. 5(a) which indicates that on average the areas of the bases of the jets which are co-temporal with local peaks in the E_f-H budgets of the AR are statistically larger than the areas of those that have no significant imprint in the evolution of the E_f -H budgets.

4. Conclusions

Throughout the observations, the E_f and H budgets of the AR were below established thersholds which, if crossed, the AR is likely to erupt. The time profiles of the E_f and H showed discrete localized peaks. Eight such peaks in each of the E_f and H curves (all well beyond uncertainties) occurred co-temporally with jet events produced in the AR. These local helicity peaks can reasonably be attributed to the jet events because no other type of eruptive activity was registered in the AR. Furthermore, their pairing with E_f localized peaks supports the same conclusion for the origin of the simultaneous E_f peaks.

The jets associated with localized peaks in the E_f and H budgets of the AR are distinguished from the other AR jets by their larger areas of their bases as well as by their longer durations. It is also interesting that these major jets are also associated with local peaks in the time profiles of the normalized free magnetic energy and helicity parameters.

The free magnetic energy and helicity losses associated with the jets are in the ranges of (1.1-6.9) x 10^{29} erg and (0.5-7.1) x 10^{40} Mx^2, respectively. These values are one to two orders of magnitude smaller than the relevant changes associated with CMEs. There are no previous explicit reports based on observations about helicity changes directly associated with jets. The percentage losses associated with the jets are significant: 9-57% for the normalized free magnetic energy and 13-76% for the normalized helicity.

This is the first report where changes in the magnetic free energy and helicity budgets of an AR are registered with such clarity with jet activity. Green et al. (2022) were the first to report jet activity in intervals when the helicity index attains large values. In our study the close synchronization of localized E_f and H peaks with jet events allowed us to estimate, for the first time, the free magnetic energy and helicity budgets associated with individual jet events.

Acknowledgements

AN, SP, KM, VA, and AAN acknowledge support by the ERC Synergy Grant (GAN: 810218) "The Whole Sun". AN thanks R.H. Cameron and A.S. Brun for useful discussions.

References

Georgoulis, M. K., Tziotziou, K., & Raouafi, N.-E. 2012, ApJ, 759, 1
Green, L. M., Thalmann, J. K., Valori, G., et al. 2022, ApJ, 937, 59
Linan, L., Pariat, É., Moraitis, K., Valori, G., & Leake, J. 2018, ApJ, 865, 52
Liokati, E., Nindos, A., & Georgoulis, M. K. 2023, A&A, 672, A38
Liokati, E., Nindos, A., & Liu, Y. 2022, A&A, 662, A6
Pariat, E., Wyper, P. F., & Linan, L. 2023, A&A, 669, A33
Tziotziou, K., Georgoulis, M. K., & Raouafi, N.-E. 2012, ApJ, 759, L4